Reduction in Tension and Stiffening of Lipid Membranes in an Electric Field Revealed by X-Ray Scattering

Arnaud Hemmerle,[1,*] Giovanna Fragneto,[2] Jean Daillant,[3] and Thierry Charitat[1,†]
[1]UPR 22/CNRS, Institut Charles Sadron, Université de Strasbourg, 23 rue du Loess, BP 84047 67034 Strasbourg Cedex 2, France
[2]Institut Laue-Langevin, 71 avenue des Martyrs, BP 156, 38042 Grenoble Cedex, France
[3]Synchrotron SOLEIL, L'Orme des Merisiers, Saint-Aubin, BP 48, F-91192 Gif-sur-Yvette Cedex, France
(Received 5 January 2016; published 2 June 2016)

The effect of ac electric fields on the elasticity of supported lipid bilayers is investigated at the microscopic level using grazing incidence synchrotron x-ray scattering. A strong decrease in the membrane tension up to 1 mN/m and a dramatic increase of its effective rigidity up to 300 k_BT are observed for local electric potentials seen by the membrane $\lesssim$1 V. The experimental results are analyzed using detailed electrokinetic modeling and nonlinear Poisson-Boltzmann theory. Based on a modeling of the electromagnetic stress, which provides an accurate description of the bilayer separation versus pressure curves, we show that the decrease in tension results from the amplification of charge fluctuations on the membrane surface whereas the increase in bending rigidity results from the direct interaction between charges in the electric double layer. These effects eventually lead to a destabilization of the bilayer and vesicle formation. Similar effects are expected at the tens of nanometers length scale in cell membranes with lower tension, and could explain a number of electrically driven processes.

DOI: 10.1103/PhysRevLett.116.228101

Electric fields can be used to destabilize lipid bilayers as in the electroformation process, the most popular method to form large unilamellar vesicles [1], or to manipulate the shape of vesicles [2–4]. Beyond biosensor applications and the investigation of the fundamental mechanical, dynamical, and binding properties of membranes using impedance spectroscopy or dielectric relaxation [5], the strong influence of electric fields on lipid membrane behavior is also used in numerous applications in cell biology, biotechnology, and pharmacology [6,7] such as cell hybridization [8], electroporation [9], electrofusion [10], and electropermeabilization [11]. All these effects imply a strong deformation of the membranes in the field, the understanding of which in terms of elastic properties is therefore of prime importance [12]. Theoretically, the effect of electric fields on membrane tension has been investigated in Ref. [13], which was extended to bending rigidity in Refs [14–18].

When placed in an electric field $\mathbf{E}$, charges of opposite sign will accumulate at both sides of a membrane, which can be seen as a capacitor with surface charge densities $\Sigma_\pm$ [see Fig. 1(a)], allowing one to calculate the normal component of the electromagnetic stress $(\Sigma_+^2 - \Sigma_-^2)/\epsilon_m$ [19]. For a flat membrane, a direct consequence is electrostriction: at equilibrium, the elastic response of the membrane (Young modulus $\sim 10^7$–10^8 Pa [5,20]) balances the electrostatic pressure [21]. Beyond this simple effect, membrane fluctuations modify the boundary conditions for the electric field, leading to a subtle coupling between electrostatics and membrane elasticity. Because of the membrane finite thickness d_m, a bending deformation induces surface element variations of opposite sign on both interfaces leading to a net local charge of the bilayer [see Fig. 1(a), bottom]. For a given surface mode $z_q \exp(i\mathbf{q}\cdot\mathbf{r})$, the surface charge density fluctuations are given by $\delta\Sigma_\pm = \mp\epsilon_m E_m d_m q^2 z_q \exp(i\mathbf{q}\cdot\mathbf{r})$, where ϵ_m is the membrane permittivity, E_m is the field seen by the membrane, and $q^2 z_q$ is the local curvature. Calculating the work of the electromagnetic stress leads to $\delta W \sim -\epsilon_m d_m E_m^2 q^2 |z_q|^2$. As $q^2|z_q|^2$ is the increase in area of the fluctuating membrane, this means that there is a negative correction to the free energy, equivalent to a negative (destabilizing) contribution Γ_m to the membrane surface tension γ [13,19]. Similar effects occur in the electric double layer leading to a total correction $\Gamma_{\rm el} = \Gamma_m + \Gamma_{\rm DL}$, where $\Gamma_{\rm DL}$ is the usually smaller correction coming from the electrical double layer [15–19]. Taking into account nonlinear effects in the electric double layer we have

$$\Gamma_m = -\epsilon_m d_m E_m^2 = -\frac{\epsilon_m}{d_m}\left[V_{\rm loc} - \frac{4k_BT}{e}\ln\left(\frac{1+c}{1-c}\right)\right]^2, \quad (1)$$

where $V_{\rm loc}$ is the local electric potential seen by the bilayer and the double electric layer, lower than the applied potential [Fig. 1(b)]. $0 < c < 1$ is a dimensionless parameter depending on the Debye length κ_D^{-1} and voltage, saturating to 1 for either high salt concentration or high voltage because of nonlinear effects in the double electric layer [15,16,19]. Further development in powers of q gives contributions in q^4 [4,15–17], corresponding to a positive correction $K_{\rm el} = K_m + K_{\rm DL}$ to the membrane bending rigidity κ: bending brings the charges closer and increases the electrostatic repulsion [see Fig. 1(a), bottom part]. Consistently, the

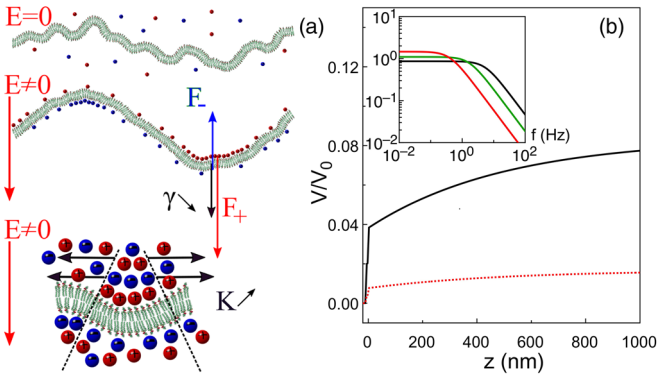

FIG. 1. Schematic representation of the effect of the electric field (a). Top: freely fluctuating bilayer. Middle: the interaction between the induced charges and the external electric field leads to an electric force that is amplifying the undulation, acting as a destabilizing negative surface tension. Bottom: bending brings the charges closer increasing the electrostatic interactions, mainly in the electric double layer (black arrows) and leads to an increase in the bending rigidity. Calculated electric potential as a function of the distance for 10 Hz (black solid curve) and 50 Hz (red dotted line) (b). The inset of (b) shows the local voltage at the membrane boundaries as a function of frequency and for different Debye lengths $\kappa_D^{-1} = 800$ nm (red curve), 300 nm (green curve), and 150 nm (black curve) using $d_m = 5$ nm. $z = 0$ corresponds to the middle plane of the floating bilayer.

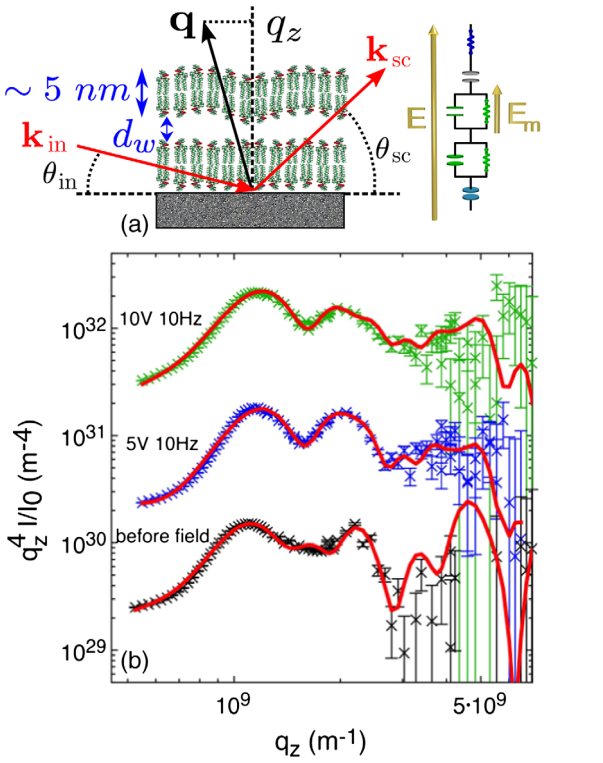

FIG. 2. Schematic view of the experiment and electrokinetic model of the supported bilayers (a). The incident beam at grazing incidence (direction $\mathbf{k}_{in}$) is scattered in direction $\mathbf{k}_{sc}$, giving access to in-plane fluctuations. The off-specular reflectivity curves and the associated best fits (b).

largest correction is now due to the thick double layer and is proportional to κ_D^{-1}:

$$K_{DL} = 4\epsilon_w \left(\frac{k_B T}{e}\right)^2 \kappa_D^{-1} \frac{c^2(3-c^2)}{1+c^2}, \tag{2}$$

where ϵ_w is the permittivity of water.

The model system we have used consisted of two supported bilayers of DSPC ($L-\alpha$ 1,2-distearoyl-sn-glycero-3-phosphocholine, Avanti Polar Lipids, Lancaster, Alabama) deposited on ultraflat silicon substrates [Fig. 2(a)] [22]. All the experiments were performed in the fluid phase at 58 °C. The first bilayer serves as a spacer to reduce the interaction between the floating second bilayer and the substrate and keeps it free to fluctuate [23,24]. A potential was applied between a Cu layer deposited at the back of the thick Si substrate and an Indium-Tin-Oxide (ITO) coated glass plate mounted parallel to the substrate, 0.5 cm from the membrane.

We used a 27 keV x-ray beam (wavelength $\lambda = 0.0459$ nm) at the CRG-IF beamline of the European Synchrotron Radiation Facility (ESRF) in an off-specular geometry described in Fig. 2(a) [25]. The grazing angle of incidence is kept fixed ($\theta_{in} = 0.7$ mrad), below the critical angle for total external reflection $\theta_c \simeq 0.85$ mrad as this allows easy background subtraction, and θ_{sc} is scanned in the plane of incidence [24,26]. In all experiments, the incident beam was 500×20 μm and the reflected intensity was defined using a 20 mm $\times$ 200 μm slit at 210 mm from the sample and a 20 mm $\times$ 200 μm slit at 815 mm from the sample and recorded using a NaI (Tl) scintillator.

Off-specular scattering is sensitive to both the static deformation and thermal fluctuations of bilayers. In the limit of small amplitudes, and the simple case of a single bilayer in an interaction potential U, the scattered intensity is $I_{sc} \propto \langle z_q z_{-q} \rangle$, with the fluctuation spectrum $\langle z_q z_{-q} \rangle = k_B T / h(\mathbf{q})$ and

$$h(\mathbf{q}) = U'' + \gamma q^2 + \kappa q^4. \tag{3}$$

The Hamiltonian of the system is given by $\mathcal{H} = \sum_q \mathcal{H}(\mathbf{q}) = \sum_q h(\mathbf{q}) |z_q|^2$. The fitting of the scattering curves, accounting for both thermal fluctuations and the static roughness induced by the substrate [27] (following the procedure described in detail in Refs. [23,26]), gives access to the bilayer electron density profile, γ, κ, and U''. Different scattering curves are presented in Fig. 2(b) and in the Supplemental Material [25], showing that high voltage differences, up to 10 V, can be applied to the cell without destroying the membrane, but strongly affecting its fluctuations. Figure 3 summarizes the main findings of this Letter. We clearly observe an electrostriction effect on the structural properties. The thickness d_w of the water

layer in between the two lipid bilayers decreases with the electric field [Fig. 3(a)]. Depending on the voltage and frequency, we also observe large negative corrections to the tension $\Gamma_{el} = \gamma_{(V=0)} - \gamma$ [up to 1 mN/m, Figs. 3(c) and 3(d)] and positive corrections to the bending stiffness $K_{el} = \kappa - \kappa_{(V=0)}$ [up to a few hundreds of k_BT, Figs. 3(e) and 3(f)]. The measured values $\gamma_{(V=0)} = 0.5$–1 mN/m and $\kappa_{(V=0)} = 15k_BT$–$20k_BT$ are in good agreement with known values for DSPC bilayers [26].

Analyzing our results first requires us to determine the local voltage drop V_{loc} seen by the bilayer. To this end, we model the system electrokinetics by solving the Poisson-Nernst-Planck equations, generalizing the model of Ziebert *et al.* [16] to the double supported bilayer [Fig. 2(a)] [19]. The only unknown parameter is the Debye screening length κ_D^{-1}, which might slightly depend on the dissolved carbon dioxide and fixes the conductivity of the solution [30]. Whereas $\kappa_D^{-1} = 960$ nm in pure water, it is reduced to 150 nm for normal atmospheric conditions. As the scattering curves were recorded 5 to 10 h after sample preparation, which can influence the Debye length, $\kappa_D^{-1} = 150$, 300 and 800 nm were used in the analysis. With these values and a single diffusion coefficient $D = 7.5 \times 10^{-9}$ m^2/s for all ions [31], the effective membrane resistance, lower than its intrinsic resistance, ranges from 20 to 300 $\Omega \cdot$ cm^2. The system behaves as a low-pass filter with a cutoff frequency determined by the bulk solution conductance R_B^{-1} and the electric double layer capacitance per unit area C_{DL} [inset of Fig. 1(b)], the highest resistance and capacitance in the system, respectively. Depending on the Debye length, $R_B = 0.5$–10 M$\Omega \cdot$ cm^2 and $C_{DL} = 0.04$–0.18 μF/cm^2, leading to cutoff frequencies of 0.2 Hz for $\kappa_D^{-1} = 150$ nm to 3 Hz for $\kappa_D^{-1} = 800$ nm. Accordingly, the voltage drop at the membrane increases from less than $0.01V_0$ at 50 Hz to $\approx 0.04V_0$ at 10 Hz, where V_0 is the ac field applied to the membrane [Fig. 2(a)].

First discussing electrostriction, the most compressible part in the system is the water layer in between the two lipid bilayers and the electromagnetic stress is balanced by the interbilayer potential. By plotting the electrostatic pressure Π [19] as a function of the interbilayer water thickness d_w [Fig. 3(a)], all points fall on a master curve obtained for both the natural entropic repulsion between bilayers [24] and the osmotic stress, either applied on floating bilayers [24] or multilayer stacks [28], demonstrating that the local electromagnetic stress is well described by our model. We also report in Fig. 3(b) the number of water molecules per lipids n_w [32] as a function of the pressure Π. Similar curves obtained when the pressure is osmotically applied on a floating bilayer [24] and on multilayer stacks [29] are also presented, clearly demonstrating that the floating bilayers behave the same way irrespective of how the mechanical stress is applied and keep their integrity under the applied electric field.

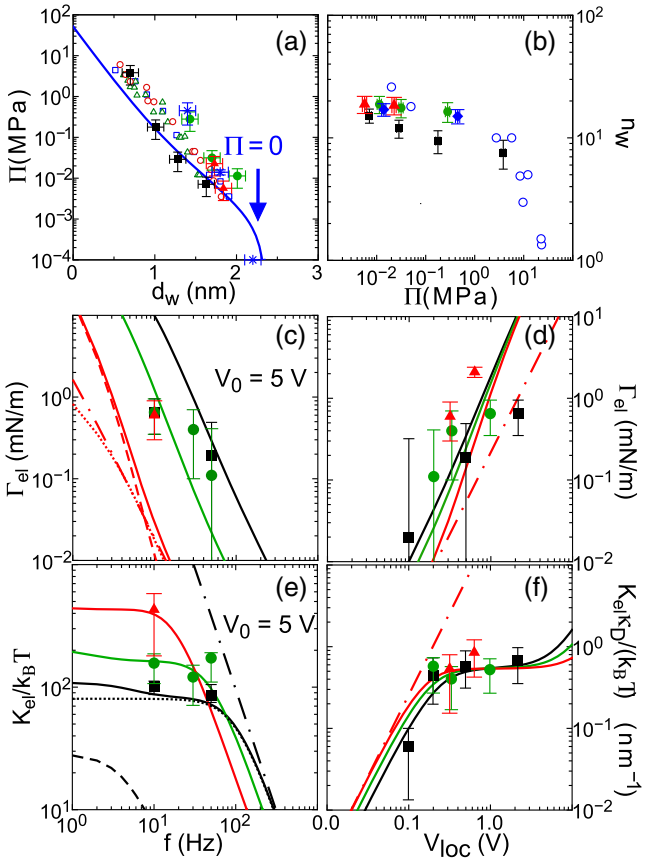

FIG. 3. Effect of an ac field on a supported bilayer. Filled symbols are data from this work. The black squares, green circles, and red triangles correspond to different experiments. The solid lines correspond to the full electrostatic contribution (Poisson-Boltzmann theory) to Γ_{el} and K_{el}, which can be decomposed into a membrane contribution (dotted line) and an electric double layer contribution (dashed line). The linear Debye-Hückel theory is shown as dashed-dotted lines. $\kappa_D^{-1} = 800$ nm (red curves), $\kappa_D^{-1} = 300$ nm (green curves), and $\kappa_D^{-1} = 150$ nm (black curves). Mechanical pressure as a function of distance (a). The blue stars are from Ref. [24] where the pressure was applied by osmotic stress on similar double bilayers. The empty symbols are from Ref. [28] (osmotic stress on multilayer stacks). The solid line is calculated after Ref. [24] using dispersive, electrostatic, and entropic contributions to the interbilayer potential. Number of water molecules per lipid n_w as a function of electrostatic pressure Π (b). The blue circles were obtained by NMR spectroscopy for osmotically stressed 1,2-dimyristoyl-sn-glycero-3-phosphocholine multilayer stacks [29]. Electrostatic contribution to the membrane tension Γ_{el} as a function of frequency for a fixed voltage $V_0 = 5$ V (c) and as a function of the local voltage V_{loc} at the membrane (d). Electrostatic contribution to the membrane rigidity K_{el} as a function of frequency for a fixed voltage $V_0 = 5$ V (e) and $K_{el}\kappa_D/k_BT$ as a function of the local potential difference V_{loc} (f).

The frequency dependence of the correction to the membrane tension Γ_{el} is plotted in Fig. 3(c) for $V_0 = 5$ V, where a $\approx \omega^{-2}$ decay is observed. The origin of this purely electrokinetic effect lies in the impossibility to charge the

membrane above the cutoff frequency of the low bandpass filter formed by the electric double layer capacitor and bulk water resistor due to the finite mobility of ions in the water. By plotting Γ_{el} as a function of the local electric field V_{loc}, we observe a good agreement between data and theoretical predictions with Γ_{el} exhibiting a roughly $\propto V_{loc}^2$ dependence [Fig. 3(d)].

The increase in bending rigidity K_{el} is plotted as a function of frequency for $V_0 = 5$ V in Fig. 3(e) and as a function of V_{loc} in Fig. 3(f). Both curves exhibit a more complex behavior than the Γ_{el} curves, which can be attributed to nonlinear effects due to the large voltage drop at the membrane with $eV/k_BT \simeq 1$ [Fig. 1(b)]. In contrast with the linear theory, which exhibits the expected ω^{-2} behavior, the low-frequency plateau seen for both the experimental data and the nonlinear theory in Fig. 3(e) comes from saturation effects in the electric double layer. By plotting the data as a function of V_{loc}, which allows one to decouple the microscopic and electrokinetic effects, all $K_{el}\kappa_D$ values indeed fall on a master curve with a saturation from 0.5 V [see Fig. 3(f)]. This is in remarkable agreement with the theory, which predicts a saturation value of K_{el} proportional to the Debye length [16], and fully consistent with the expectation that a thicker layer is more difficult to bend. As κ_D also fixes independently cutoff frequencies via the water conductivity, the analysis is clearly consistent. However, we must point out that despite its remarkable description of our data, the theory of Ref. [15] is for a single bilayer in a symmetric environment, unlike the experimental conditions used here. The electroformation technique uses a similar electric field to destabilize membranes and fabricate giant unilamellar vesicles. The stability limit of the bilayers can be calculated using $h(\mathbf{q}) = 0$, and is drawn in Fig. 4(a) for two different values of the potential second derivative ($U'' = 3 \times 10^{11}$ and 3×10^{12} J · m^{-4}). It clearly shows that our x-ray experiments are performed in the stability domain but close to instability conditions. With the aim of observing destabilization, we have applied an electric field on a single supported bilayer on an Indium-Tin-Oxide coated glass slide under similar conditions. We observed by fluorescence microscopy the formation of giant unilamellar vesicles above and close to the main transition temperature T_m [Fig. 4(b)]. Small vesicles of diameter ≈ 5 μm are the dominant population at short times ($t \sim 1$–10 min) and grow with time to reach a diameter of 10–30 μm. Interestingly, the initial size we find here is consistent with the instability in the bilayer fluctuation spectra evidenced by x-ray scattering.

The effect of ac fields on supported floating bilayers has been investigated by x-ray off-specular scattering. In a consistent set of experimental data strongly supported by an established theoretical model, we have evidenced both a dramatic decrease in the membrane tension, possibly down to negative values, and a strong increase in the bilayer bending rigidity. We demonstrate that the effect on tension

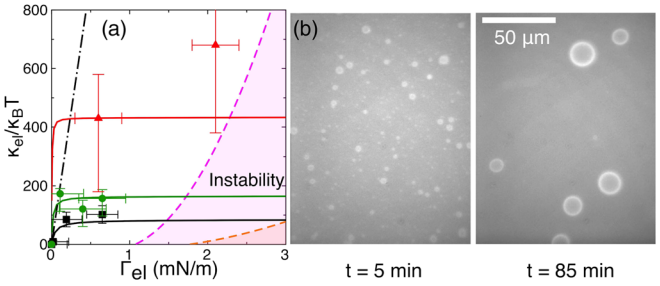

FIG. 4. Γ_{el} as a function of K_{el} (a). The destabilization limits for $U'' = 10^{12.5}$ and $10^{11.5}$ J · m^{-4} are given as light and dark pink domains, respectively. Vesicle formation under an electric field (5 V, 5 Hz) from a single supported bilayer of 1,2-dipalmitoyl-sn-glycero-3-phosphocholine (b). Observation by fluorescence microscopy at 5 min (left) and 85 min (right) after the application of the field.

results from an amplification of charge fluctuations at the membrane. The effect on rigidity comes from couplings inside the electric double layer, and can only be understood by using the full nonlinear Poisson-Boltzmann theory. The effect of voltage and ac field frequency has been characterized. The competition between the stabilizing effect on bending rigidity (mainly acting at length scales ≤ 0.5 μm) and the destabilizing effect on tension (at length scales ≥ 0.5 μm) leads to ≈ 1 μm vesicle formation as observed. This detailed understanding can now be used for further analysis of the effect of electric fields on biological membranes. For cell membranes that have a smaller rigidity ($\sim 1k_BT$–$10k_BT$) than our model membrane, destabilization is expected to occur at length scales $\simeq 50$ nm and could explain the effect of low electric fields in processes like electroendocytosis.

The authors wish to thank L. Malaquin and S. Micha for assistance during the experiments and L. Malaquin, D. Lacoste, and F. Ziebert for useful discussions. Support from the Agence Nationale de la Recherche through projects LabEx NIE (Grant No. ANR-11-LABX-0058 NIE) and support facilities at the ILL for sample preparation are gratefully acknowledged.

*Present address: Max Planck Institute for Dynamics and Self-Organization (MPIDS), Göttingen 37077, Germany.
†thierry.charitat@ics-cnrs.unistra.fr

[1] M. Angelova and D. Dimitrov, Liposome electroformation, Faraday Discuss. Chem. Soc. **81**, 303 (1986).
[2] K. A. Riske and R. Dimova, Electro-deformation and poration of giant vesicles viewed with high temporal resolution, Biophys. J. **88**, 1143 (2005).
[3] R. Dimova, N. Bezlyepkina, M. Domange Jordo, R. Knorr, K. Riske, M. Staykova, P. Vlahovska, T. Yamamoto, P. Yang, and R. Lipowsky, Vesicles in electric fields: Some novel aspects of membrane behavior, Soft Matter **5**, 3201 (2009).

[4] P. F. Salipante, M. L. Shapiro, and P. M. Vlahovska, Electric field induced deformations of biomimetic fluid membranes, Procedia IUTAM **16**, 60 (2015).
[5] T. Hianik, Electrostriction and dynamics of solid supported lipid films, Rev. Mol. Biotechnol. **74**, 189 (2000).
[6] M. Zhao, B. Song, J. Pu, T. Wada, B. Reid, G. Tai, F. Wang, A. Guo, P. Walczysko, Y. Gu, T. Sasaki, A. Suzuki, J. Forrester, H. Bourne, C. Devreotes, P. N. McCaig, and J. Penninger, Electrical signals control wound healing through phosphatidylinositol-3-oh kinase-γ and PTEN, Nature (London) **442**, 457 (2006).
[7] U. Zimmermann, Electrical breakdown, electropermeabilization and electrofusion, in *Reviews of Physiology*, Vol. 105 (Springer, Berlin, 1986), pp. 175–256.
[8] U. Zimmermann and G. Neil, *Electromanipulation of Cells* (CRC Press, Cleveland, 1996).
[9] R. S. Son, K. C. Smith, T. R. Gowrishankar, P. T. Vernier, and J. C. Weaver, Basic features of a cell electroporation model: Illustrative behavior for two very different pulses, J. Membr. Biol. **247**, 1209 (2014).
[10] L. Rems, M. Usaj, M. Kanduser, M. Rebersek, D. Miklavcic, and G. Pucihar, Cell electrofusion using nanosecond electric pulses, Sci. Rep. **3**, 3382 (2013).
[11] P. Vernier, Y. Sun, and M. Gundersen, Nanoelectropulse-driven membrane perturbation and small molecule permeabilization, BMC Cell Biol. **7**, 37 (2006).
[12] P. M. Vlahovska, Voltage-morphology coupling in biomimetic membranes: dynamics of giant vesicles in applied electric fields, Soft Matter **11**, 7232 (2015).
[13] P. Sens and H. Isambert, Undulation Instability of Lipid Membranes under Electric Field, Phys. Rev. Lett. **88**, 128102 (2002).
[14] F. Ziebert, M.-Z. Bazant, and D. Lacoste, Effective zero-thickness model for a conductive membrane driven by an electric field, Phys. Rev. E **81**, 031912 (2010).
[15] F. Ziebert and D. Lacoste, A poisson boltzmann approach for a lipid membrane in an electric field, New J. Phys. **12**, 095002 (2010).
[16] F. Ziebert and D. Lacoste, Planar lipid bilayer in an electric field: Membrane instability, flow field, and electrical impedance, Adv. Planar Lipid Bilayers Liposomes **14**, 63 (2011).
[17] T. Ambjörnsson, M. A. Lomholt, and P. L. Hansen, Applying a potential across a biomembrane: Electrostatic contribution to the bending rigidity and membrane instability, Phys. Rev. E **75**, 051916 (2007).
[18] B. Loubet, P. L. Hansen, and M. A. Lomholt, Electromechanics of a membrane with spatially distributed fixed charges: Flexoelectricity and elastic parameters, Phys. Rev. E **88**, 062715 (2013).
[19] See Supplemental Material at http://link.aps.org/supplemental/10.1103/PhysRevLett.116.228101 for more details on modeling.
[20] L. Picas, F. Rico, and S. Scheuring, Direct measurement of the mechanical properties of lipid phases in supported bilayers, Biophys. J. **102**, L01 (2012).
[21] G. C. Fadda, D. Lairez, Z. Guennouni, and A. Koutsioubas, Peptide Pores in Lipid Bilayers: Voltage Facilitation Leads for a Revised Model, Phys. Rev. Lett. **111**, 028102 (2013).
[22] T. Charitat, E. Bellet-Amalric, G. Fragneto, and F. Graner, Adsorbed and free lipid bilayers at the solid-liquid interface, Eur. Phys. J. B **8**, 583 (1999).
[23] J. Daillant, E. Bellet-Amalric, A. Braslau, T. Charitat, G. Fragneto, F. Graner, S. Mora, F. Rieutord, and B. Stidder, Structure and fluctuations of a single floating lipid bilayer, Proc. Natl. Acad. Sci. U.S.A. **102**, 11639 (2005).
[24] A. Hemmerle, L. Malaquin, T. Charitat, S. Lecuyer, G. Fragneto, and J. Daillant, Controlling interactions in supported bilayers from weak electrostatic repulsion to high osmotic pressure, Proc. Natl. Acad. Sci. U.S.A. **109**, 19938 (2012).
[25] See Supplemental Material at http://link.aps.org/supplemental/10.1103/PhysRevLett.116.228101 for more details on experimental methods.
[26] L. Malaquin, T. Charitat, and J. Daillant, Supported bilayers: Combined specular and diffuse x-ray scattering, Eur. Phys. J. E **31**, 285 (2010).
[27] P. S. Swain and D. Andelman, Supported membranes on chemically structured and rough surfaces, Phys. Rev. E **63**, 051911 (2001).
[28] H. I. Petrache, N. Gouliaev, S. Tristram-Nagle, R. Zhang, R. M. Suter, and J. F. Nagle, Interbilayer interactions from high-resolution x-ray scattering, Phys. Rev. E **57**, 7014 (1998).
[29] K. Mallikarjunaiah, A. Leftin, J. J. Kinnun, M. J. Justice, A. L. Rogozea, H. I. Petrache, and M. F. Brown, Solid-state ^{2}H NMR shows equivalence of dehydration and osmotic pressures in lipid membrane deformation, Biophys. J. **100**, 98 (2011).
[30] D. Haughey and J. C. Earnshaw, Studies of colloidal interactions using total internal reflection microscopy, Colloids Surf. A **136**, 217 (1998).
[31] W. M. Haynes, *CRC Handbook of Chemistry and Physics* (CRC Press, Cleveland, 2013).
[32] J. F. Nagle and M. C. Wiener, Relations for lipid bilayers: Connections of electron density to other structural quantities, Biophys. J. **55**, 309 (1989).